JOURNAL OF CATALYSIS **161,** 87–95 (1996)
ARTICLE NO. 0165

Alkaline-Metal Doped MoO_3/TiO_2 Systems: Structure of Supported Molybdates

C. Martin, I. Martin, V. Rives, and P. Malet*

*Dpto. Química Inorgánica, Universidad de Salamanca, Facultad de Farmacia, 37007 Salamanca, Spain; and *Dpto. Química Inorgánica, Instituto de Ciencia de Materiales, Universidad de Sevilla, CSIC, 41012 Sevilla, Spain*

Received December 19, 1994; revised December 13, 1995; accepted February 2, 1996

The structure of molybdenum oxocompounds formed in TiO_2-supported MoO_3 systems doped with alkaline metals have been studied by X-ray diffraction (XRD) and Fourier transform infrared (FT-IR) and X-ray absorption (XAS) spectroscopies. XRD, FT-IR, and XAS data give a detailed picture of the structure of molybdenum oxocompounds formed in these systems. Mo atoms are mostly octahedrally coordinated in an undoped TiO_2 support, as a dispersed MoO_3 phase. However, a high fraction of molybdenum cations are in tetrahedral coordination after the addition of Li, Na, or K as dopants. Thus, only MoO_4^{2-} species exist in the 1 wt% Li-doped sample in the form of crystalline Li_2MoO_4, while tetrahedrally and octahedrally coordinated molybdenum form dispersed $Mo_2O_7^{2-}$ chains in the 1 wt% Na- and K-doped systems. Octahedral polymolybdates, $Rb_2Mo_3O_{10} \cdot H_2O$ and $Rb_2Mo_4O_{13}$, whose structures are based in $[MoO_6]$ units forming chains, are the species detected in the 1 wt% Rb-doped sample. Increasing the molybdenum content in K-doped samples favors formation of octahedral species, although in this case the structure of the supported phase is affected by the impregnation steps during the preparation of the sample.

INTRODUCTION

Systems where molybdenum oxide is dispersed on a support are widely applied as catalysts in several heterogeneous catalytic reactions (1). The structure of the supported phase and the surface acidity can be considered as the main factors controlling the catalytic properties of such systems (2). Both properties, acidity and structure of the supported phase, can be changed by adding doping agents that thus are able to modify the activity and selectivity of molybdena in catalytic reactions. Doping supported molybdena samples with alkaline metal cations induces changes in their reactivity (3), the nucleophilic character of the surface (4), or the reducibility of supported molybdena (5). In a previous paper (6) some of us have studied the surface acidity of MoO_3/TiO_2 systems doped with alkaline cations (Li, Na, K, Rb), concluding that the incorporation of alkaline cations leads to a decrease in the surface acidity and of the ratio between the concentration of Brønsted and Lewis surface acid sites. Structural changes after alkali doping have been also reported (5, 7–9). Thus, changes in the oxygen coordination of molybdenum atoms from octahedral to tetrahedral after doping with K or Cs (5) are suggested by a decrease in the reducibility of molybdena and are definitely shown by X-ray absorption (XAS) spectroscopy in Na doped MoO_3/TiO_2 samples (5, 9). X-ray diffraction (XRD) and Fourier transform-infrared (FT-IR) data suggest the formation of polymolybdates on the surface of K-doped MoO_3/TiO_2 samples (8), with only two IR bands at 948 and 902 cm^{-1} at high molybdena contents. Bands at these wave numbers were previously ascribed to octahedral molybdates (10–13). However, the chemistry and structures of alkaline molybdates are complex (14), and it is difficult to ascertain the molybdate structure from IR data only. For bulk molybdates different structures are known, and basic MoO_x units with four or six oxygen atoms around the molybdenum cation form chains, layers, or clusters. Thus, IR spectra of K-doped, low molybdena loaded samples show several weak absorption bands (8) between 980 and 850 cm^{-1}. Similar IR bands have been assigned to octahedral molybdates (10–13), but in Na-doped MoO_3/TiO_2 samples (5) they arise from a mixture of isolated MoO_4^{2-} tetrahedra and $Mo_2O_7^{2-}$ chains, formed by tetrahedral and octahedral MoO_x units.

This paper reports the structural characterization of MoO_3/TiO_2 samples doped with alkaline metal cations (Li, Na, K, Rb) by means of X-ray diffraction, Fourier transform infrared spectroscopy, temperature programmed reduction, and X-ray absorption spectroscopy. Results are discussed on the basis of the known structures of bulk alkaline molybdates.

EXPERIMENTAL

1. Samples. Supports were obtained from TiO_2 (P-25, Degussa). After calcination at 770 K overnight to remove adsorbed organic impurities, a 1 wt% of the alkaline metal cation M (M = Li, Na, K, Rb) was incorporated to TiO_2 by impregnation with aqueous solutions of $LiNO_3$, NaOH,

0021-9517/96 $18.00

KNO_3, or $RbNO_3$, respectively. After drying and calcination at 770 K for 3 h, the doped supports were impregnated with an ammonium heptamolybdate (AHM) solution in the amount necessary to achieve one theoretical geometric monolayer of MoO_3 (5.9 wt% Mo), as calculated from the BET surface area of the support (53 ± 2 m^2 g^{-1}) and the surface occupied by a "molecule" of MoO_3 (15×10^4 pm^2 (15)). In some cases, the effect of higher molybdena or alkaline loadings were investigated. A second batch of K-doped samples was prepared by coimpregnation of the TiO_2 support with an aqueous solution containing both KNO_3 and AHM in order to ascertain the effect of the preparation procedure. All the impregnated products were dried at 383 K for 24 h and calcined at 770 K in air, a temperature high enough to achieve total decomposition of AHM to MoO_3.

2. Experimental procedures. **XRD** profiles were recorded in a Philips PW 1070 instrument, using Ni-filtered Cu$K\alpha$ radiation ($\lambda = 154.05$ pm). **Nitrogen adsorption** measurements at 77 K for surface area determination were carried out in a conventional high vacuum pyrex system (residual pressure 10^{-4} N m^{-2}) where pressure changes were monitored with a MKS pressure transducer. **FT-IR spectra** were recorded in a Perkin-Elmer FT-IR 1730 spectrometer using KBr disks, with a nominal resolution of 4 cm^{-1} and averaging 100 spectra. A KBr disk with the same weight of the unloaded support was used to record the background spectrum in order to cancel all the absorption bands due to the support. **Temperature programmed reduction** (TPR) profiles were recorded, at a heating rate of 10 K/min, in a conventional apparatus with a catharometric detector using 50 ml/min of 5% H_2/Ar as carrier gas. The amount of sample reduced (ca. 160 mg) corresponds to 100 μmol of Mo, thus ensuring good resolution under the experimental conditions used (16). **XAS** data were collected at 77 K on wiggler station 9.2 at the Daresbury Synchrotron Radiation Source (U.K.) with an electron ring running at 2 GeV and 210–230 mA. Monochromatization was obtained with a double silicon crystal monochromator working at the (220) reflection, which was detuned 50% to minimize higher harmonics. The measurements were carried out in transmission mode using optimized ion chambers as detectors. Supported samples were ground and homogenized, and the precalculated amounts of the sample powders were pressed into a self-supporting wafer with absorbance 2.5 above the Mo–K edge (20,005 eV). Reference compounds were diluted with boron nitride and prepared in the same way. Mo–K spectra were measured at liquid nitrogen temperature under a helium atmosphere to avoid water condensation. At least three scans were recorded and averaged in order to obtain the experimental spectra. The EXAFS function ($\chi(k)$) was obtained from the experimental X-ray absorption spectrum by conventional procedures (17). EXAFS data analysis and handling were performed by using the program package NEWEXAFS. Experimental backscattering amplitude and phase functions for Mo–Mo and Mo–O absorber-backscatterer pairs were obtained from the XAFS of MoS_2 and $Na_2MoO_4 \cdot 2H_2O$ (5), both measured under helium at 77 K.

RESULTS

Specific surface area values (S_{BET}) as well as the anatase contents in the support (as determined by the equation given by Criado and Real (18)) are given in Table 1. All the samples were prepared by successive impregnation and the MoO_3 content equals one theoretical monolayer. They are named as Mo/Ti/Alk, where Alk stands for the alkaline element added to the support. With the exception of the molybdena loaded Li-doped sample, where a strong rutilization is detected, calculated anatase contents are similar to that of the parent support. Impregnation procedures followed by calcination slightly decrease the specific surface area of the support, this decrease being higher for the molybdena loaded samples and for the Li-doped system.

The XRD pattern for MoO_3–TiO_2 doped with 1 wt% Li (Fig. 1a) shows that crystalline Li_2MoO_4 (JPCDS card 12/763) is formed in this sample, since diffraction lines that can be ascribed to this compound appear in addition to those of anatase and rutile. The Li/Mo atomic ratio in this sample is 2.3, high enough to allow a complete reaction of molybdena with litium to form the molybdate. As shown in Fig. 1a, the intensity of diffraction lines ascribed to Li_2MoO_4 is only slightly modified when increasing the Li content to 3 wt%, thus suggesting that all the molybdenum has already reacted to form Li_2MoO_4 in the 1% Li sample. The main effect of a higher Li content while the molybdenum loading is constant is a strong increase in the intensity of the line appearing at $2\theta = 18°$. This line also appears in the

TABLE 1

Samples Studied in This work[a]

Sample	S_{BET} (m^2 g^{-1})	% Anatase
TiO_2	53	55
Ti/Li	39	53
Ti/Na	47	55
Ti/K	50	55
Ti/Rb	53	54
Mo/Ti	42	52
Mo/Ti/Li	19	12
Mo/Ti/Na	39	50
Mo/Ti/K	44	53
Mo/Ti/Rb	47	53

[a] Unless otherwise stated, data in this table and following are for samples containing one theoretical monolayer of MoO_3 and 1 wt% of alkaline metal.

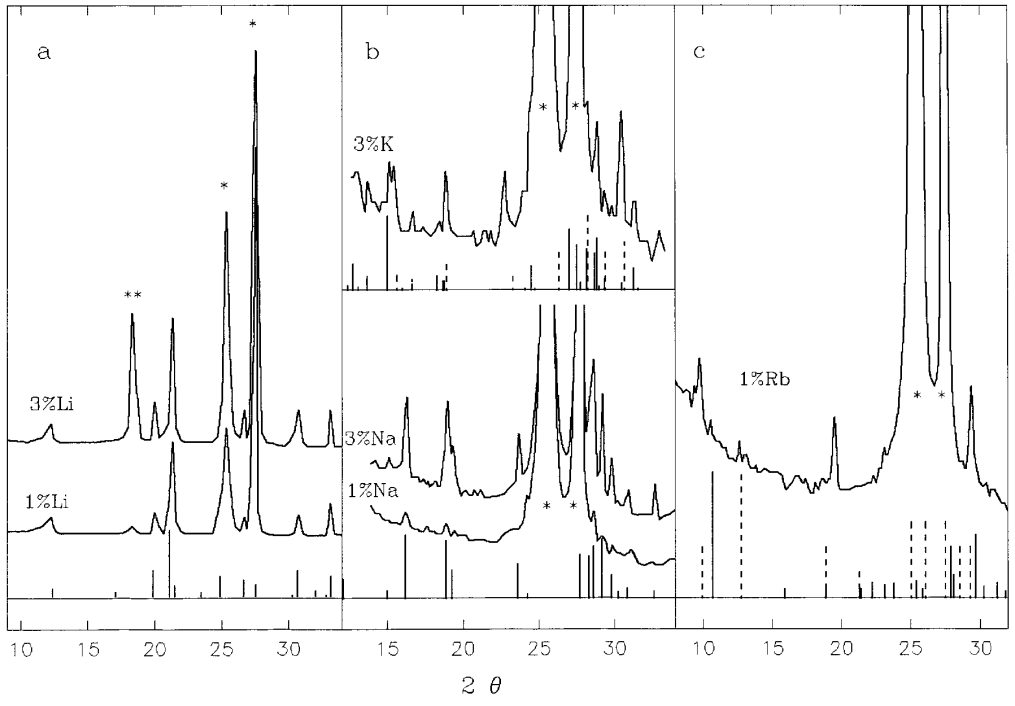

FIG. 1. XRD patterns for one monolayer MoO_3/TiO_2 samples doped with alkaline metals: (a) Li-doped samples, bars indicate diffraction lines of Li_2MoO_4; (b) Na- and K-doped samples, bars indicate diffraction lines for $Na_2Mo_2O_7$, $K_2Mo_2O_7$ (solid bars), and K_2MoO_4 (dashed bars); (c) Rb-doped sample, bars indicate diffraction lines for $Rb_2Mo_3O_{10} \cdot H_2O$ (solid bars) and $Rb_2Mo_4O_{13}$ (dashed bars). TiO_2 lines are marked by (*) in all the diagrams, while (**) stands for a line already present in the TiO_2–Li support.

molybdenum-free 1% Li-doped TiO_2 support and should be therefore ascribed to the formation of a Li–Ti–O compound.

Figure 1b shows the XRD pattern for samples with one monolayer of supported molybdena doped with Na or K. For the 1% Na-doped sample diffraction lines that could be ascribed to Mo–O–Alk phases are very weak and hardly distinguished over the noise level. The intensity of these lines increases when increasing the Na content and the diffraction pattern of $Na_2Mo_2O_7$ (JPCDS card 22/906) clearly appears for the 3 wt% Na sample. The additional presence of $Na_2MoO_4 \cdot 2H_2O$ cannot be discarded since intense diffraction lines for this compound at 361, 331, 317, 306, and 298 pm overlap either with lines for sodium dimolybdate (314, 306, 300 pm) or with strong lines of the TiO_2 support (351 pm for anatase and 325 pm for rutile). The behavior of K-doped samples is very similar, and when the K content is 1 wt% lines that could be ascribed to molybdenum oxocompounds are very weak in the XRD pattern (not shown), also increasing their intensity for the 3% K sample where a mixture of crystalline $K_2Mo_2O_7$ and K_2MoO_4 is detected (JPCDS cards 36/347 and 24/880; see Fig. 1b). These data indicate that a high fraction of molybdenum is undetected by XRD in the samples doped with a 1 wt% of Na or K, and therefore is present as an amorphous phase in these samples.

The diffraction pattern of the 1% Rb-doped Mo–Ti–Rb sample (Fig. 1c) shows weak diffractions that coincide either with the most intense lines of crystalline $Rb_2Mo_3O_{10} \cdot H_2O$ (JPCDS card 35/325) or with lines reported for $Rb_2Mo_4O_{13}$ (JPCDS card 24/957), thus indicating the simultaneous formation of both crystalline compounds.

TPR profiles of supported molybdena have been shown (19, 20) to be very sensitive to the structure of the supported phase. As shown in Fig. 2, the TPR profile of Mo/Ti/Rb is very similar to that recorded for undoped MoO_3/TiO_2, thus suggesting that MoO_x species must be similar in both samples. FT-IR spectra of these samples (Table 2) are also similar, and only a broad absorption band at ca. 960 cm^{-1}, ascribed (21) to noncrystalline MoO_3, is detected for the undoped sample. This band, also recorded as a shoulder in the FT-IR spectrum of Mo/Ti/Rb, appears as a well defined peak at higher molybdena loadings (22). TPR profiles for K- and Na-doped systems (Figs. 2c and 2d) are almost identical and are characterized by the relative high intensity of the reduction process at ca. 1100 K. This fact could be explained either by the agglomeration of MoO_3 crystals or by the formation of compounds containing $[MoO_4]$ tetrahedral units since both species show reduction processes at temperatures higher than 973 K (5). The lack of the characteristic absorption band for MoO_3 in the IR spectra of K- and Na-doped samples discards the presence of crystalline MoO_3,

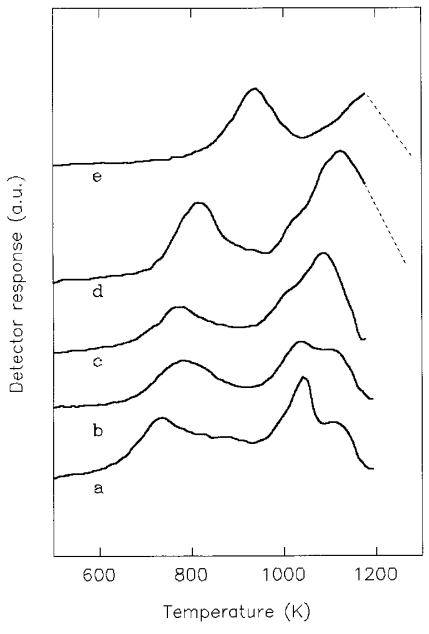

FIG. 2. TPR profiles of one monolayer supported samples: (a) undoped MoO_3/TiO_2, (b) Mo/Ti/Rb, (c) Mo/Ti/K, (d) Mo/Ti/Li.

in agreement with XRD results, while the presence of several absorption bands in the 960–850 cm^{-1} range (Table 2) suggests the coexistence of MoO_4^{2-} species (band at ca. 900 cm^{-1} (5)) and $Mo_2O_7^{2-}$ anions (bands at 938–948, 920–923, 871–881 cm^{-1} (5)). The TPR profile for the Li-doped sample (Fig. 2e) shows a clear change. The reducibility of molybdenum compounds is much lower than in the undoped support or in the Na-, K-, and Rb-doped samples, as shown by the increase in the onset of the reduction process and the high temperature of the reduction maxima. This change is ascribed to the formation of Li_2MoO_4, detected in this sample by XRD. The presence of MoO_4^{2-} anions forming this molybdate in sample Mo–Ti–Li explains its FT-IR spectrum (Table 2) with only two absorption bands at 894 and 862 cm^{-1}, similar to those found for bulk $Na_2MoO_4 \cdot 2H_2O$ (5).

TABLE 2

IR Bands in Supported Samples and Reference Materials

Sample	ν (cm^{-1})						
Mo/Ti	960						
MoO_3	989					879	
Mo/Ti/Li					894		862
$Na_2MoO_4 \cdot 2H_2O$					900		858
Mo/Ti/Na[a]		938	923	910	897		
Mo/Ti/K		948	920	904	893[b]	871	
$Na_2Mo_2O_7$		943	923	905		881	864

[a] Ill defined bands.
[b] Shoulder.

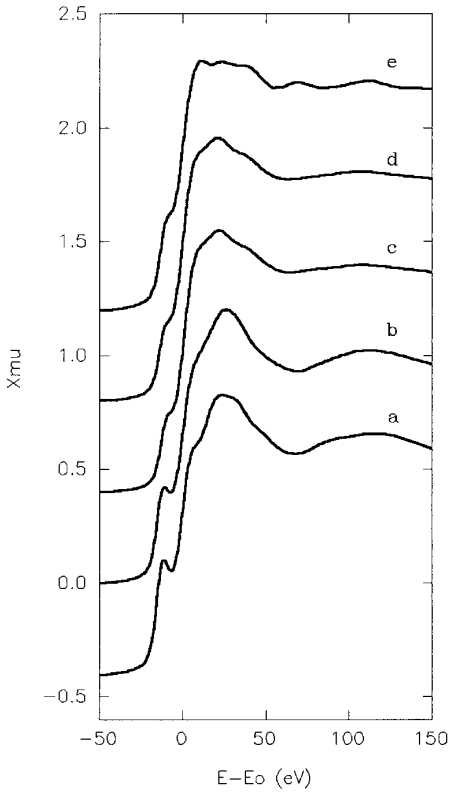

FIG. 3. XANES Spectra at the Mo–K edge: (a) $Na_2MoO_4 \cdot 2H_2O$, (b) Mo/Ti/Li, (c) Mo/Ti/Na, (d) Mo/Ti/K, (e) MoO_3.

Information about the local surrounding of molybdenum atoms in the MoO_3/TiO_2-doped samples can be obtained by XAS spectroscopy. As shown in Fig. 3, the different local coordination of molybdenum atoms in bulk MoO_3 and $Na_2MoO_4 \cdot 2H_2O$ (distorted octahedral and regular tetrahedra, respectively) accounts for differences in their XANES spectra at the Mo–K edge. Thus, while in $Na_2MoO_4 \cdot 2H_2O$ a defined pre-edge peak appears before the main absorption edge, this peak is merely a shoulder in MoO_3. Therefore, the intensity of this pre-edge peak can be taken as an indicative of the amount of molybdenum atoms in tetrahedral coordination. As shown in Fig. 3 for our samples, the local coordination of these atoms in samples Mo/Ti/Na and Mo/Ti/K is very similar, and mainly octahedral, while a large percentage of tetrahedral [MoO_4] units should exist in sample Mo/Ti/Li, which XANES spectrum is almost identical to that recorded for $Na_2MoO_4 \cdot 2H_2O$.

EXAFS spectra for alkaline doped MoO_3/TiO_2 samples are shown in Fig. 4, and their associated k^3-weighted Fourier transforms are shown in Fig. 5. Data for crystalline MoO_3 and $Na_2MoO_4 \cdot 2H_2O$ have been included for comparison. The radial distribution function derived from the EXAFS of sodium molybdate contains only a main peak (1.25 Å, phase shift uncorrected) that, according to its structure as determined by X-ray diffraction (23), has been assigned

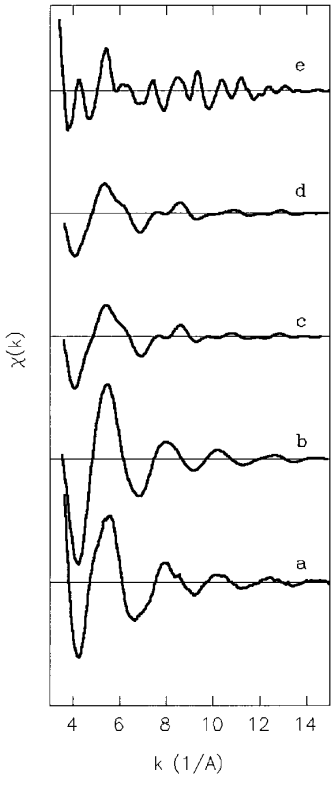

FIG. 4. Unfiltered EXAFS oscillations at the Mo–K edge: (a) $Na_2MoO_4 \cdot 2H_2O$, (b) Mo/Ti/Li, (c) Mo/Ti/Na, (d) Mo/Ti/K, (e) MoO_3.

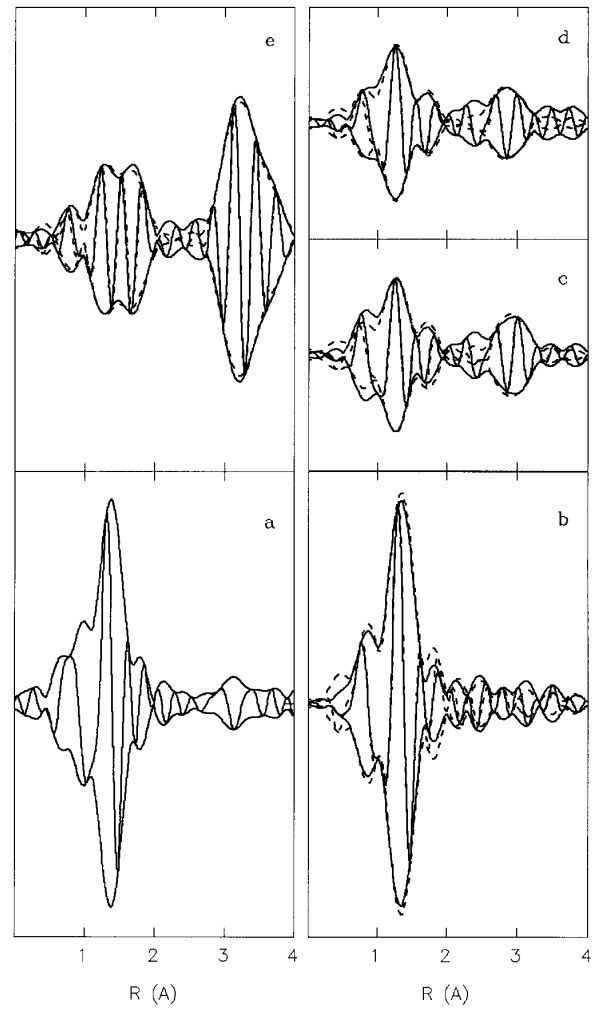

FIG. 5. k^3-weighted Fourier transforms of EXAFS spectra: (a) $Na_2MoO_4 \cdot 2H_2O$, (b) Mo/Ti/Li, (c) Mo/Ti/Na, (d) Mo/Ti/K, (e) MoO_3. Solid lines, experimental data. Dashed lines, best fit functions; Δk = 4–13.5 $Å^{-1}$ in all the Fourier transforms.

(5, 9) to four oxygen neighbors at 1.772 Å. EXAFS oscillations for MoO_3 are much more complicated, giving rise in the uncorrected k^3-weighted FT to two overlapped peaks at 1–2 Å and another one at 3.1 Å. The first two maxima has been assigned (5, 9) to Mo–O contributions in the distorted [MoO_6] octahedra that built the MoO_3 structure while the peak at 3.1 Å is mainly due to Mo–Mo absorber–backscatterer pairs. The [MoO_6] distorted octahedron can be simulated (5, 9) by equal number of oxygen atoms at three different distances yielding a total coordination number of 6.0 up to 2.5 Å, in good agreement with crystallographic data (23b). Higher shells contributions can be modeled (5) by Mo–Mo pairs at three different distances yielding a total coordination number of 6.8 also in agreement, within the experimental error, with Mo–Mo distances and coordination numbers as determined from crystallographic data (23b). EXAFS parameters for bulk MoO_3 are summarized in Table 3.

In agreement with the above conclusions from application of other experimental techniques, the EXAFS spectrum for the 1% Li sample is very similar to that for $Na_2MoO_4 \cdot 2H_2O$ and can be fitted with only one Mo–O shell at 1.77 Å (fit parameters in Table 3). O/Mo coordination number and the lack of Mo–Mo coordination shells show that in this sample most of the molybdenum atoms are tetrahedrally coordinated after the addition of the dopant to the titania support, appearing as monomeric MoO_4^{2-} anions.

Meanwhile, Fourier transforms for the Na- and K-doped samples are almost identical. Comparison of these FT with those for reference compounds shows that the regular structure at long range present in MoO_3 (peak at 3 Å) has almost vanished in the Mo–Ti–Alk samples. The local order of oxygen atoms around Mo leads to maxima centered at 1.25 Å that seem to be intermediate between those for the known structures of the crystalline compounds, thus suggesting that both types of coordination for molybdenum atoms—distorted [MoO_6] octahedron and regular [MoO_4] tetrahedron—coexist in these samples. The spectra have been analyzed following a procedure previously described (5) that simulates first shell Mo–O contributions by using three different Mo–O distances (1.7, 1.96, 2.26 Å). The first distance averages the 1.77 Å bond of the tetrahedral

TABLE 3

Results of EXAFS Analysis

Sample	Shell	R (Å)	N	$\Delta\sigma^2 \times 10^3$	ΔE° (eV)	% Td
$Na_2MoO_4 \cdot 2H_2O$[a]	O	1.772	4.0			100
MoO_3	O	1.69	1.9	1.7	8.5	
	O	1.96	2.1	0.3	6.7	
	O	2.26	2.0	5.9	4.2	
	Mo	3.45	1.9	1.2	1.2	
	Mo	3.71	2.4	2.6	19.6	
	Mo	4.03	2.5	3.4	9.3	
Mo/Ti/Li	O	1.76	4.1	0.3	2.8	100
Mo/Ti/Na	O	1.72	2.7	3.1	7.1	
	O	1.95	1.7	3.7	8.8	
	O	2.21	1.2	9.1	4.4	30
	Mo	3.28	1.2	2.9	14.2	
Mo/Ti/K	O	1.72	2.7	3.1	7.0	
	O	1.95	1.7	3.7	8.8	
	O	2.21	1.2	9.1	4.3	30
	Mo	3.25	1.0	2.9	21.0	

[a] EXAFS reference compound for Mo–O bonds (parameters from Ref. (23)). Estimated errors for coordination numbers (N) and shell distances (R) are ±15% and ±0.02 Å, respectively.

structure with the shortest bond length (1.69 Å) of the octahedral units, while longer bond lengths (1.96, 2.26 Å) appear only in the distorted [MoO_6] octahedra. Increasing the relative fraction of molybdenum atoms in tetrahedral coordination will lead to increased values of the coordination number at ca. 1.7 Å (N_1), and to a decrease of the total Mo–O coordination number (N_t). The N_1/N_t ratio can be used to determine the fraction (x) of [MoO_4] units through the relationship $N_1/N_t = (2 + 2x)/(6 - 2x)$. The results obtained upon this first shell analysis were taken as the starting point for a more complete analysis up to 4 Å in r-space. Mo–Mo contributions were added by starting with shell parameters as obtained for MoO_3. After refining the amplitudes, the shell radii as well as the ΔE° shifts were taken into the refinement. Best fit parameters are included in Table 3 and fit results are plotted in Fig. 5.

Results for Mo–O first shell contributions indicate that the fraction of molybdenum atoms in tetrahedral coordination is equal within the experimental error in Na or K-doped samples (ca. 30%). Regarding Mo–Mo shells, signals due to Mo–Mo distances are still present, although coordination numbers are much lower than those found for crystalline MoO_3. Mo–Mo bond lengths (3.26 ± 0.02 Å) are shorter than those found in bulk MoO_3. Short Mo–Mo bond lengths, reported for $Mo_7O_{24}^{6-}$ (24), are also found in other polymolybdate anions (see below), and can be taken as an evidence of the formation of polymolybdate species over the surface of these samples.

Some of us have previously reported (8) effects of the preparation procedure on the surface properties of K-doped MoO_3/TiO_3 when the MoO_3 content exceeds the monolayer. Results reported in this paper indicate that for samples containing two monolayer of MoO_3 the simultaneous impregnation (coimpregnation) with potassium and molybdenum salts favors the formation of potassium polymolybdates, which were the only species detected even at low K contents (1%, w/w). Thus, while crystalline MoO_3 was detected by XRD and FT-IR in a two monolayer sample prepared by successive impregnation, a similar sample prepared by coimpregnation shows XRD lines for the supported phase at 895, 689, 521, 381, and 293 pm, which indicate the formation of $K_2Mo_3O_{10}$ (diffraction lines at 684, 520, 383, and 295 pm) and potassium heptamolybdate (intense diffraction lines at 891 and 696 pm). The FT-IR spectrum of the latter sample shows only two bands at 948 and 902 cm^{-1}. Samples prepared by both procedures but with lower MoO_3 contents were identical. Figure 6A shows XANES spectra of 1% K– MoO_3/TiO_2 samples with a MoO_3 content of two theoretical monolayer (Mo/2/Ti/K) and prepared by both impregnation procedures. While the sample prepared by successive impregnation has a XANES spectrum whose fine structure is similar to that obtained for bulk MoO_3, these features for the coimpregnated sample are closer to those recorded for Na- and K-doped one monolayer samples, thus indicating that polymolybdates are formed even at high Mo/K ratios following this preparation procedure. Mo–K edge EXAFS spectra (Fig. 6B) also confirm structural differences between the two samples prepared by either successive impregnation or coimpregnation. The shortening of Mo–Mo bond lengths ascribed to the formation of polymolybdates is evident in the coimpregnated sample, while for the sample prepared by successive impregnation the maximum at ca. 3.5 Å in the uncor-

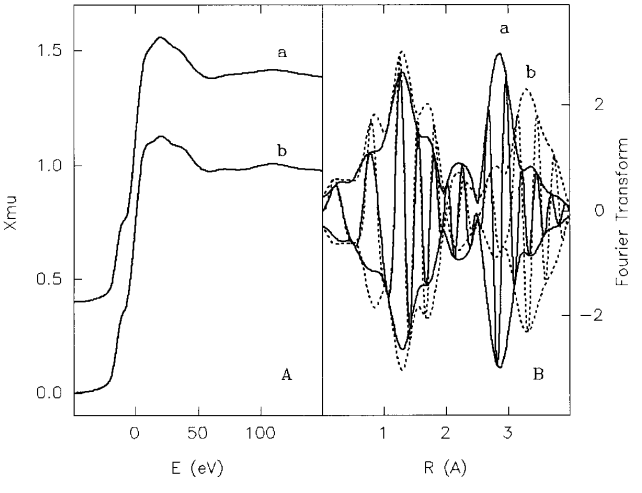

FIG. 6. Mo/2/Ti/K samples: (A) Mo–K edge Xanes spectra and (B) k^3-weighted Fourier transforms of the EXAFS oscillations ($\Delta k = 4 - 13.5$ Å^{-1}): (a) sample prepared by coimpregnation, (b) sample prepared by successive impregnation.

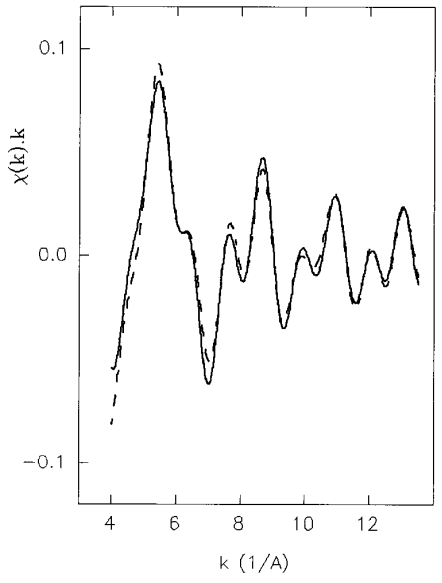

FIG. 7. Coimpregnated Mo/2/Ti/K sample: experimental EXAFS oscillations (solid line) and best fit function (dashed line).

rected k^3-Fourier transform is very similar to that reported for bulk MoO_3. EXAFS oscillations for the coimpregnated sample were fitted (Fig. 7) following the procedure above described, leading to the fit parameters collected in Table 4. A low O/Mo coordination number (1.8) at ca. 1.7 Å, a total O/Mo coordination number of 5.7, and a short Mo–Mo bond length indicate that polymolybdate species, where molybdenum cations are mainly in octahedral coordination, are formed in the two monolayer sample prepared by coimpregnation.

DISCUSSION

Recent results (5, 25) reported on the structure of dispersed MoO_x moieties formed on the surface of undoped MoO_3/TiO_2 show that molybdenum atoms are mainly in octahedral coordination, and only a small fraction of them (ca. 15%) have a tetrahedral coordination on the TiO_2 support. Present data for alkaline-doped MoO_3/TiO_2 samples indicate that when Li, Na, or K dopants are present molybdenum forms either crystalline or dispersed molybdates, leading to the presence of molybdenum cations in tetrahedral coordination. Thus, EXAFS data show that all molybdenum atoms are in tetrahedral coordination in the Mo/Ti/Li sample with a Li/Mo atomic ratio 2.3, and only short Mo–O bond lengths (1.77 Å) appear. The lack of Mo–Mo bond lengths for this sample indicates the formation of monomeric $[MoO_4]$ tetrahedra that yield a simple pattern in the infrared spectrum with two bands at 894 and 862 cm^{-1}. XRD data show that the presence of these tetrahedra is due to the formation of crystalline Li_2MoO_4 in this sample.

Meanwhile, FT-IR, TPR, and XAS data for Mo/Ti/Na and Mo/Ti/K samples are almost identical, suggesting that Mo–O–Alk phases yielding very weak XRD diffractions have a similar structure in both systems, in spite of their different Alk/Mo atomic ratios (0.7 and 0.4 for 1 wt% Na and K, respectively). Thus, EXAFS data indicate that molybdenum atoms in tetrahedral and octahedral coordination form the dispersed phase in these samples. The infrared spectra show several absorption bands in the range 850–960 cm^{-1}, which coincide with that reported for bulk $Na_2Mo_2O_7$ (5), and can be ascribed to the formation of $Mo_2O_7^{2-}$ anions. Figure 8 shows the structure of dimolybdate anions in crystalline $K_2Mo_2O_7$ and $Na_2Mo_2O_7$. Both anions have equal number of $[MoO_4]$ and $[MoO_6]$ units sharing vertex to form chains. Table 5 collects Mo–O and Mo–Mo bond lengths and coordination numbers in $Mo_2O_7^{2-}$ anions obtained from crystallographic data (26, 27). While tetrahedral units have four short Mo–O bond lengths, similar to those found in MoO_4^{2-} anions (1.77 Å), $[MoO_6]$ units are distorted, showing three different bond lengths similar to those found in

TABLE 4

Coimpregnated Mo/2/Ti/K Sample: EXAFS Parameters

Shell	R (Å)	N	$\Delta\sigma^2 \times 10^3$	ΔE° (eV)
O	1.69	1.8	0.8	14.7
O	1.96	2.2	9.3	6.7
O	2.28	1.7	11.0	1.2
Mo	3.25	1.2	1.2	14.2
Mo	3.71	0.3	0.7	20.0
Mo	4.03	0.2	0.5	4.2

Note. Estimated errors for coordination numbers (N) and shell distances (R) are ±15% and ±0.02 Å, respectively.

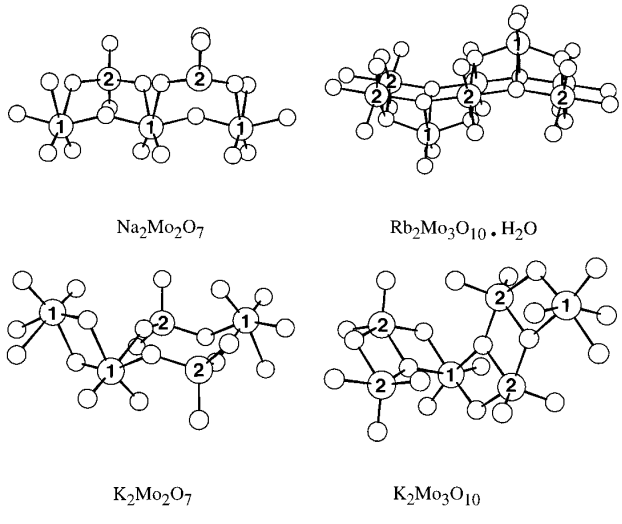

FIG. 8. Structure of chain molybdates. Labeled circles stand for Mo atoms. Unlabeled circles stand for oxygen atoms.

TABLE 5

Coordination of Molybdenum Atoms in Polymolybdate Chains[a]

Compound	Target	Mo–O bonds	Mo–Mo bonds
$Na_2Mo_2O_7$	Mo(1)	1.69 Å × 2 1.90 Å × 2 2.27 Å × 2	3.59 Å × 4
	Mo(2)	1.76 Å × 4	3.59 Å × 2
$K_2Mo_2O_7$	Mo(1)	1.75 Å × 2, 1.82 Å 2.06 Å, 2.17 Å, 2.27 Å	3.10 Å, 3.42 Å 3.78 Å
	Mo(2)	1.77 Å × 4	3.42 Å, 3.78 Å
$K_2Mo_3O_{10}$	Mo(1)	1.70 Å × 2 1.95 Å × 2 2.18 Å × 2	3.23 Å × 2 4.00 Å × 2
	Mo(2)	1.70 Å × 2 1.97 Å × 3	3.23 Å × 2 4.00 Å
$Rb_2Mo_3O_{10} \cdot H_2O$	Mo(1)	1.72 Å × 2 1.94 Å × 2 2.22 Å × 2	3.27 Å × 4
	Mo(2)		3.27 Å × 2 3.58 Å 3.80 Å × 2

[a] Derived from crystallographic data for bulk compounds (Refs. 27–29).

MoO_3. Average values of Mo–O bond lengths and total coordination numbers for these compounds are included in Table 6. Experimental Mo–O coordination numbers and bond lengths obtained from the analysis of the EXAFS spectra for Mo/Ti/Na and Mo/Ti/K samples are consistent with the presence of both dimolybdates, while the fraction of $[MoO_4]$ units (ca. 30%) suggests that dimolybdate chains coexist with octahedral molybdates, similar to those found in the undoped support. The simultaneous presence of a small amount of monomeric $[MoO_4]$ units, the only species detected in the Li-doped sample, may not be discarded from the experimental data. Mo–Mo coordination numbers are lower than those expected for the bulk compounds, thus suggesting noncrystalline dimolybdates, probably in the form of short chains. This result agrees with the low intensity of their characteristic X-ray diffraction lines in the samples doped with 1 wt% of Na or K. The formation of short dimolybdate chains, with a high degree of disorder, could account for Mo–Mo bond lengths in the supported samples (3.25–3.28 Å), shorter than those found in the crystalline dimolybdates (see Table 5).

TABLE 6

Average Distances of Oxygen Shells (*R*) and Coordination Numbers (*N*) in Crystalline Molybates

Compound	Subshell	*R* (Å)	*N*	N_t	N_1/N_t
$Na_2Mo_2O_7$	O_1	1.72	3		
	O_2	1.90	1		
	O_3	2.27	1	5	0.60
$K_2Mo_2O_7$	O_1	1.77	3.5		
	O_2	2.06	0.5		
	O_3	2.22	1	5	0.70
$K_2Mo_3O_{10}$	O_1	1.70	2		
	O_2	1.96	2.67		
	O_3	2.18	0.67	5.33	0.37
$Rb_2Mo_3O_{10} \cdot H_2O$	O_1	1.72	2		
	O_2	1.94	2		
	O_3	2.22	2	6	0.33

Note. N_t is the total O/Mo coordination number and N_1 is the number of O atoms at short Mo–O bond lengths (ca. 1.7 Å).

$Mo_2O_7^{2-}$ chains are detected in Mo–Ti–Na and Mo–Ti–K samples (Alk/Mo ratios 0.7 and 0.4, respectively), while Li_2MoO_4 is the only species found in the Mo–Ti–Li sample (Alk/Mo = 2.3). However, it should be noted here that our data previously reported (5) for a 3 wt% Na-doped MoO_3/TiO_2 sample with a Na/Mo atomic ratio 2.1 show that in this case only ca. 70% of molybdenum cations are in tetrahedral coordination, and molybdenum is forming a mixture of $Na_2Mo_2O_7$ and Na_2MoO_4. This result indicates that Li is more effective than Na, on an atomic basis, in inducing the formation of $[MoO_4]$ units.

On the other hand, increasing the molybdenum content in the two monolayer Mo/2/Ti/K samples, favors the formation of compounds with $[MoO_6]$ octahedral units. Experimental data (8) for the sample prepared by successive impregnation show that MoO_3 crystallizes on the surface. However, formation of $Mo_3O_{10}^{2-}$ and $Mo_7O_{24}^{7-}$ is favored when the sample is prepared by coimpregnation. Thus, the presence of new XRD lines over the TiO_2 diffraction pattern suggests the formation of $K_2Mo_3O_{10}$ and $K_6Mo_7O_{24}$ in this case, while EXAFS data yield a total O/Mo coordination number of 5.7, and ca. 1.8 short Mo–O bonds at 1.77 Å, indicating a negligible fraction of molybdenum cations in tetrahedral coordination. $Mo_7O_{24}^{6-}$ anions are clusters (24) formed by seven distorted $[MoO_6]$ units with Mo–Mo bond lengths in the range 3.24–3.44 Å (average Mo/Mo coordination number 3.4 at an average distance 3.30 Å). $Mo_3O_{10}^{2-}$ anions (Fig. 8) are chains formed by $[MoO_6]$ units that share edges with pentaoxocoordinated molybdenum atoms (28). Crystallographic Mo–O bond lengths (Table 5) show that in this case hexa- and pentacoordinated molybdenum atoms have short and long bond distances and, as shown in Table 6, average Mo–O bond lengths and total O/Mo coordination numbers coincide, within experimental error, with those expected for octahedral $[MoO_6]$ units. Mo–Mo distances (3.23 Å) are similar to those found in the Mo/2/Ti/K sample, as well as for the heptamolybdate anion.

Finally, TPR and FT-IR data suggest that the structure of molybdenum oxocompounds in sample Mo/Ti/Rb is similar to that previously reported for undoped MoO_3/TiO_2, where molybdenum atoms are mainly in octahedral coordination. Unfortunately, XAFS data were not measured for

this sample; however, the only species detected by XRD are $Rb_2Mo_3O_{10} \cdot H_2O$ and $Rb_2Mo_4O_{13}$, both with an octahedral coordination of molybdenum by oxygen. A crystalline MoO_3 phase, where molybdenum cations are also as $[MoO_6]$ units, that coexists with the octahedral molybdates is readily formed either by increasing the molybdena content of the sample or decreasing the Rb/Mo atomic ratios (22). FT-IR data for Rb-doped samples show that bands ascribed to isolated $[MoO_4]$ units or to octahedral–tetrahedral chains do not appear for molybdena loadings of one to two theoretical monolayers or Rb/Mo atomic ratios in the range 0.1–0.6. It should be here noted that chains in $Rb_2Mo_3O_{10} \cdot H_2O$ (29) have a structure where $[MoO_6]$ octahedra share edges (Fig. 8). The highest Mo/Mo coordination number in this structure is expected at a short bond length (3.27 Å, see Table 5). A similar description was given (5) for the supported phase in the undoped sample, where the formation of zig-zag rows containing three to eight $[MoO_6]$ units explained the low Mo–Mo coordination numbers and the preferential decrease of coordination numbers at long Mo–Mo bond lengths.

ACKNOWLEDGMENTS

Financial support from DGICYT under Projects PB93-0633 and PB92-0665 is acknowledged. Thanks are given to the staff of Daresbury Laboratory for support during XAS measurements. I.M.acknowledges a grant from Ministerio de Educatión y Ciencia (Madrid, Spain).

REFERENCES

1. Gelling, P. J., *in* "Catalysis" (G. C. Bond, and G. Webb, Eds.), Special Periodical Reports, Vol. 7, p. 105. The Royal Society of Chemistry, London, 1985.
2. Knözinger, H., *in* "Proceedings 9th International Congress on Catalysis, Calgary; 1988." (M. J. Philips and M. Ternan Eds.). Chem. Institute of Canada, Ottawa, 1988.
3. Tatsumi, T., Muramatsu, A., and Tomianaga, H., *Appl. Catal.* **27**, 69 (1986).
4. Martin, C., Martin, I., and Rives, V., *J. Catal.* **145**, 239 (1994).
5. Martin, C., Martin, I., Rives, V., and Malet, P., *J. Catal.* **147**, 465 (1994).
6. Martin, C., Martin, I., del Moral, C., and Rives, V., *J. Catal.* **146**, 415 (1994).
7. O'Young, C. L., *J. Phys. Chem.* **93**, 2016 (1989).
8. Martin, C., Mendizabal, M. C., and Rives, V., *J. Mater. Sci.* **27**, 5575 (1992).
9. Malet, P., Muñoz-Paez, A., Martin, C., Martin, I., and Rives, V., *in* "Catalysis and Surface Characterization" (T. J. Dines, C. H. Rochester, and J. Thomson, Eds.), p. 256. The Royal Society of Chemistry, Cambridge, 1992.
10. Ng, K.Y.S., and Gulari, E., *J. Catal.* **95**, 33 (1985).
11. Giordano, N., Bart, J. C. J., Castellan, S., and Vaghi, A., *in* "First International Conference on Chemistry and Uses of Molybdenum" (P. C. H. Mitchel, Ed.), p. 194. Climax Molybdenum Company, Ann Arbor, MI, 1973.
12. Nysquist, R. A., and Kagel, R. D., "Infrared Spectra of Inorganic Compounds." Academic Press, London, 1971.
13. Asmalov, G. N., and Krylov, O. V., *Kinet. Katal.* **847**, (1970).
14. Wells, A. F., "Structural Inorganic Chemistry," 5th ed. Oxford Science, London, 1984.
15. Fransen, T., Van Berge, C., and Mars, P., *in* "Preparation of Catalysts" (P. Delmon, P. A. Jacobs, and G. Poncelet, Eds.), p. 405. Elsevier, Amsterdam, 1984.
16. Malet, P., and Caballero, A., *J. Chem. Soc. Faraday Trans. I* **84**, 2369 (1988).
17. Sayers, D. E., and Bunker, B. A., *in* "X-Ray Absorption: Principles, Applications and Techniques of EXAFS, SEXAFS and XANES" (D. C. Koningsberger and R. Prins, Eds.). Wiley, New York, 1988.
18. Criado, J. M., and Real, C., *J. Chem. Soc. Faraday Trans. I* **79**, 2765 (1983).
19. del Arco, M., Carrazan, S. R. G., Martin, C., Martin, I., Rives, V., and Malet, P., *J. Mater. Chem.* **3**, 1313 (1993).
20. Valyon, J., Heyker, M., and Wenlandt, K. P., *React. Kinet. Catal. Lett.* **38**, 265 (1989).
21. Bond, G. C., Flamerz, S., and van Wijk, L., *Catal. Today* **1**, 229 (1987).
22. Martin, I., Ph.D. thesis, Universidad de Salamanca, Spain, 1993.
23. (a) Matsumoto, K., Kobayashi, A., and Sasaki, Y., *Bull. Chem. Soc. Jpn.* **48**, 1009 (1975); (b) Kihlborg, L., *Ark. Kemi* **21**, 357 (1963).
24. Structural Reports 32A, 296 (1967).
25. Shimada, H., Matsubayashi, N., Sato, T., Yoshimura, Y., and Nishijima, A., *J. Catal.* **138**, 746 (1992).
26. Lindqvist, I., *Acta Chem. Scand.* **4**, 1066 (1960).
27. Gatehouse, B. M., and Jozsa, A. J., *J. Solid State Chem.* **71**, 34 (1987).
28. Gatehouse, B. M., and Leverett, P., *J. Chem Soc. A* 1938 (1968).
29. Kreusler, H. U., Foerster, A., and Fuchs, J., *Z. Naturf. B Anorganische* **35**, 242 (1980).